Observational Study

Medicine

OPEN

A lipid metabolism-related risk signature for patients with gliomas constructed with TCGA and CGGA data

Dingqiang Meng, BM[a], Ting Liu, MM[a,*]

Abstract

Lipid metabolism affects cell proliferation, differentiation, membrane homeostasis and drug resistance. An in-depth exploration of lipid metabolism in gliomas might provide a novel direction for gliomas treatment. A lipid metabolism-related risk signature was constructed in our study to assess the prognosis of patients with gliomas. Lipid metabolism-related genes were extracted. Differentially expressed genes (DEGs) were screened, and a risk signature was built. The ability of the risk signature to predict the outcomes of patients with gliomas was assessed using the log-rank test and Cox regression analysis. The relationships between immunological characteristics, drug sensitivity and the risk score were evaluated, and the risk-related mechanisms were also estimated. Twenty lipid metabolism-related DEGs associated with the patient prognosis were included in the risk signature. The survival rate of high-risk patients was worse than that of low-risk patients. The risk score independently predicted the outcomes of patients. Immunological parameters, drug sensitivity, immunotherapy benefits, and numerous molecular mechanisms were significantly associated with the risk score. A lipid metabolism-related risk signature might effectively assess the prognosis of patients with gliomas. The risk score might guide individualized treatment and further clinical decision-making for patients with gliomas.

Abbreviations: CGGA = The Chinese Gliomas Genome Atlas, CIBERSORT = cell-type identification by estimating relative subsets of RNA transcripts, DEGs = differentially expressed genes, ESTIMATE = estimation of stromal and immune cells in malignant tumor tissues using expression data, GBM = glioblastoma, GSEA = gene set enrichment analysis, GTEx = genotype-tissue expression, ICIs = immune checkpoint inhibitors, KEGG = Kyoto encyclopedia of genes and genomes, LGG = low-grade gliomas, PPI = protein–protein interaction, TCGA = The Cancer Genome Atlas, TIDE = tumor immune dysfunction and exclusion, TMB = tumor mutational burden, TME = tumor immune microenvironment.

Keywords: gliomas, lipid metabolism, risk score, tumor immune

1. Introduction

Metabolic reprogramming, immune evasion, and inflammation are considered 3 important hallmarks of malignant tumors.[1] In terms of metabolic reprogramming, in addition to alterations in glycolysis,[2] the dysregulation of lipid metabolism has been identified as one of the emerging hallmarks of abnormal metabolism in tumor cells, particularly the increase in de novo lipid synthesis, which promotes tumor aggressiveness.[3,4] Lipid metabolism affects cell proliferation, differentiation and membrane homeostasis.[5] The alterations that occur in lipid metabolism provide energy for the rapid growth of tumor cells, and lipid metabolites help protect tumor cells from damage caused by harmful external environments.[6–8] Lipid metabolism was identified to be dysregulated in multiple cancers. Lipid-associated synthetases were inversely associated with survival in patients with glioblastoma (GBM), breast cancer, ovarian cancer, bladder cancer, and lung cancer.[9,10] Moreover, the acidic microenvironment induced by hypoxia might maintain the survival of cancer cells, such as lung cancer and breast cancer cells, by increasing lipid metabolism.[11] Lipid metabolism was also associated with drug resistance in cancers, and leptin produced by adipocytes contributes to resistance to 5-fluorouracil in pancreatic cancer and colorectal cancer.[12,13] Based on these findings, the roles of lipid metabolism in malignant tumors have received extensive attention.

Gliomas are the most common primary intracranial malignant tumors, and their incidence is increasing.[14] The world health organization classifies gliomas into 4 grades: grade I is benign, grades II to III are low-grade gliomas (LGGs), and grade IV is GBM. Gliomas are intractable, despite the use of multiple treatment approaches; unfortunately, high-grade gliomas have a poor prognosis (median survival of patients with GEM was 16 months), and even some patients with LGGs do not respond to

The authors have no conflicts of interest to disclose.

The datasets generated during and/or analyzed during the current study are publicly available.

This study did not require ethical approval. We will disseminate our findings by publishing the results in a peer-reviewed journal.

[a] *Department of Neurology, Traditional Chinese Medicine Hospital, ChongQing, China.*

* *Correspondence: Ting Liu, Department of Neurology, Traditional Chinese Medicine Hospital. Tongliang. Chongqing. Chongqing, China. post code: 402560. China (e-mail: Dr_TingLiu@163.com).*

How to cite this article: Meng D, Liu T. A lipid metabolism-related risk signature for patients with gliomas constructed with TCGA and CGGA data. Medicine 2022;101:36(e30501).

Received: 29 April 2022 / Received in final form: 2 August 2022 / Accepted: 4 August 2022

http://dx.doi.org/10.1097/MD.0000000000030501

treatments, mainly due to the highly heterogeneous and invasive nature of gliomas.[15–17] Furthermore, gliomas have a high recurrence rate and are prone to progress to higher grades. Therefore, novel tumor markers for the diagnosis and treatment of gliomas are urgently needed. Several recent studies have suggested that gliomas exhibit abnormal lipid metabolism.[18–20] Therefore, an in-depth exploration of lipid metabolism in gliomas might provide a novel direction for the treatment of gliomas.

In the current study, gliomas data from The Cancer Genome Atlas (TCGA) and Genotype-Tissue Expression (GTEx) were used to identify differentially expressed lipid metabolism-related genes in normal and tumor tissues, and a risk signature was constructed that could accurately assess the prognosis of patients with gliomas. Data from the Chinese gliomas genome atlas (CGGA) were utilized to validate the risk signature. Subsequently, the relationships between the risk score and the tumor immune microenvironment (TME), immune cell infiltration, immune checkpoints, drug susceptibility, and biological function were further evaluated (Fig. 1).

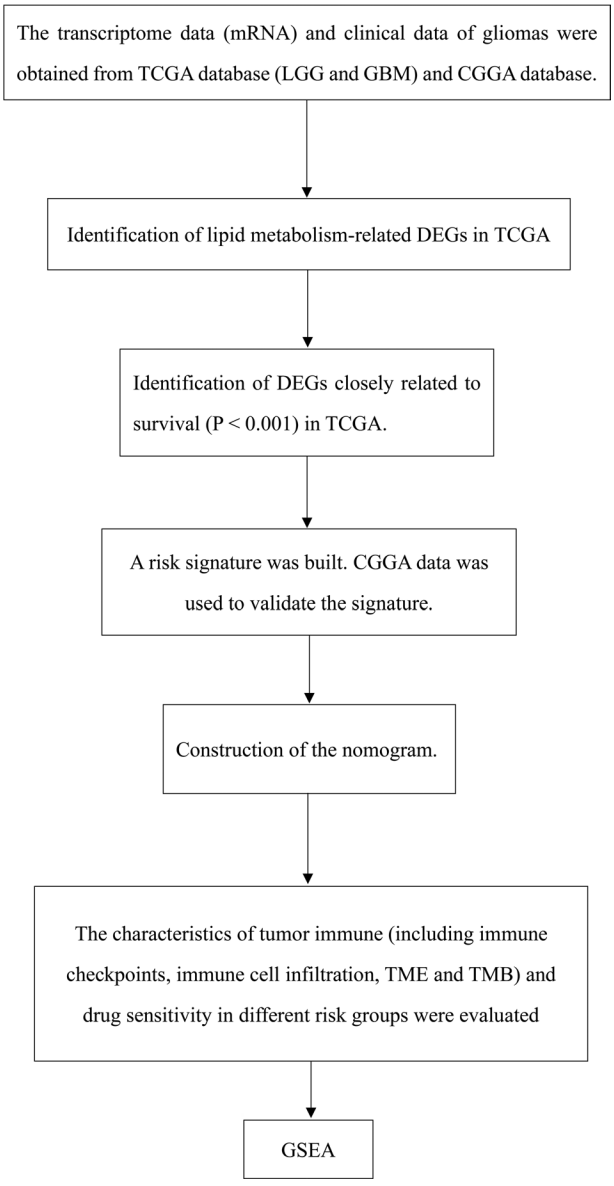

Figure 1. Flowchart of current research. CGGA = Chinese gliomas genome atlas, DEGs = differentially expressed genes, GBM = glioblastoma, GSEA = gene set enrichment analysis, LGG = low-grade gliomas, TCGA = The Cancer Genome Atlas, TMB = tumor mutational burden, TME = tumor microenvironment.

2. Methods

2.1. Collection of gliomas data

Transcriptome data, mutation data and corresponding clinical data for gliomas (LGG and GBM) were downloaded from TCGA database, and messenger RNA data from normal brain tissues were obtained from the GTEx database. After removing unavailable data, 1854 tissue-specific transcriptome data, including data from 1152 normal brain tissues and 697 tumor tissues, and clinical data from 1187 patients were included. The normalized merge data from TCGA and GTEx databases were used as the training set. Transcriptome data and clinical data for 1018 gliomas in the CGGA database were included as the validation set. The gene set "GOBP_LIPID_METABOLIC_PROCESS" was obtained from the molecular signatures database, and 1388 lipid metabolism-related genes were extracted. The tumor immune dysfunction and exclusion (TIDE) database (http://tide.dfci.harvard.edu/) was used to predict the immune checkpoint inhibitor (ICI) response in patients with gliomas.[21]

2.2. Screening of differentially expressed genes (DEGs) and construction of a risk signature

DEGs were identified using the limma package in R. The screening thresholds were adjusted P values <.05 and |log [fold change]| > 1. The screened DEGs were included in a univariate Cox analysis, and those with a P value <.001 were considered associated with the prognosis. Then, the selected genes were incorporated into least absolute shrinkage and selection operator Cox regression model, and the obtained coefficients for each gene were utilized to calculate the risk score (glmnet package in R). The cutoff value for the high-risk group and low-risk group was the median risk score. The difference in survival between the high-risk group and the low-risk group was tested by constructing survival curves (log-rank test), and the accuracy of the risk score in predicting the prognosis of patients with gliomas was visualized by constructing receiver operating characteristic curves using the R time receiver operating characteristic package. Univariate and multivariate Cox analyses were performed to assess whether risk scores could serve as an independent predictor of the prognosis of gliomas patients. A nomogram was built using the R rms package, and the corresponding calibration curve was used to evaluate the degree of agreement between the clinical results predicted by the nomogram and the actual clinical results. The CGGA dataset was used to validate the aforementioned risk score. Genes included in the risk signature were used to construct a protein–protein interaction (PPI) network through the STRING database (https://cn.string-db.org), and then the hub genes in the network were identified. Coexpression between the selected genes was also further investigated and visualized with a correlation heatmap. Images of immunohistochemical staining for the proteins encoded by the selected genes were retrieved from the Human Protein Atlas database (https://www.proteinatlas.org/) to preliminarily verify gene expression.

2.3. TME and immune cell infiltration

The transcriptome data obtained from the tumor samples were used to evaluate the status of the TME (stromal score, immune score and tumor purity) using the Estimation of Stromal and Immune cells in Malignant Tumor tissues using Expression data (ESTIMATE) algorithm,[22] and the infiltration levels of 22 specific immune cells were evaluated using the Cell-type Identification by Estimating Relative Subsets of RNA Transcripts (CIBERSORT) algorithm.[23] The relationships between the stromal score, immune score, tumor purity and 22 immune cell infiltration levels and the risk score were assessed.

2.4. Drug sensitivity

The relationships between the risk score and the susceptibility to 6 common chemotherapeutic drugs (bleomycin, cisplatin, docetaxel, doxorubicin, gemcitabine, and paclitaxel) were assessed using the R pRRophetic package.[24] The tumor mutational burden (TMB), which was calculated using the maftools R package, was used as one of the criteria for evaluating the efficacy of ICIs therapy. The relationship between the risk score and the TMB was estimated. Differences in the effects of ICIs between the 2 risk groups predicted by the TIDE database were assessed using the chi-square test.

2.5. Biological functions

A gene set enrichment analysis (GSEA) was performed to analyze risk score-related functions and pathways. The "c2.cp.kegg.v7.4.symbols.gmt" and "c5.go.v7.4.symbols.gmt" sets were downloaded from the Molecular Signatures Database. A nominal *P* value (*P* value) <.05 and a false discovery rate *Q* value (*Q* value) <0.25 were considered significant. GSEA was completed using GSEA software version 4.0.

2.6. Statistical analysis

The Wilcoxon rank sum test was used to compare the significance of differences between the 2 groups. The survival analysis was performed using the survival package in R. For correlation analyses, the Spearman test was used. All statistical calculations were performed with R software (version 4.1.3).

3. Results

3.1. Identification of DEGs and establishment of a risk signature

The clinical information obtained from TCGA and CGGA datasets were shown in Tables 1 and 2. In TCGA dataset, 139

Table 1

Characteristics of the gliomas patients obtained from the TCGA database.

Basic information		TCGA (n = 1187)
Age		52 (median)
Gender	Female	492
	Male	695
Grade	G2	291
	G3	264
	G4	272
	NA	1
Radiotherapy status	Yes	821
	No	252
	NA	114

TCGA = The Cancer Genome Atlas.

Table 2

Characteristics of the gliomas patients obtained from the CGGA database.

Basic information		CGGA (n = 1018)
Age		42 (median)
Gender	Female	417
	Male	601
Grade	G2	291
	G3	334
	G4	388
	NA	5
Radiotherapy status	Yes	754
	No	202
	NA	62
Chemotherapy status	Yes	679
	No	272
	NA	67
IDH1 mutation status	Wildtype	435
	Mutant	531
	NA	52
1p19q codeletion status	Codeletion	212
	Non-codeletion	728
	NA	78
MGMT methylation status	Un-methylated	376
	Methylated	472
	NA	170

CGGA = Chinese glioma genome atlas, IDH1 = isocitrate dehydrogenase 1, MGMT = O6-methylguanine-DNA methyl-transferase.

lipid metabolism-related DEGs were screened (tumor vs normal), including 108 downregulated genes and 31 upregulated genes (Fig. 2A and B). According to the univariate Cox analysis, 45 DEGs were significantly associated with the prognosis of patients with gliomas ($P < .001$) (Fig. 3A). The selected genes were included in the least absolute shrinkage and selection operator Cox regression model, and the risk score was calculated from the coefficients for each gene (Fig. 3B and

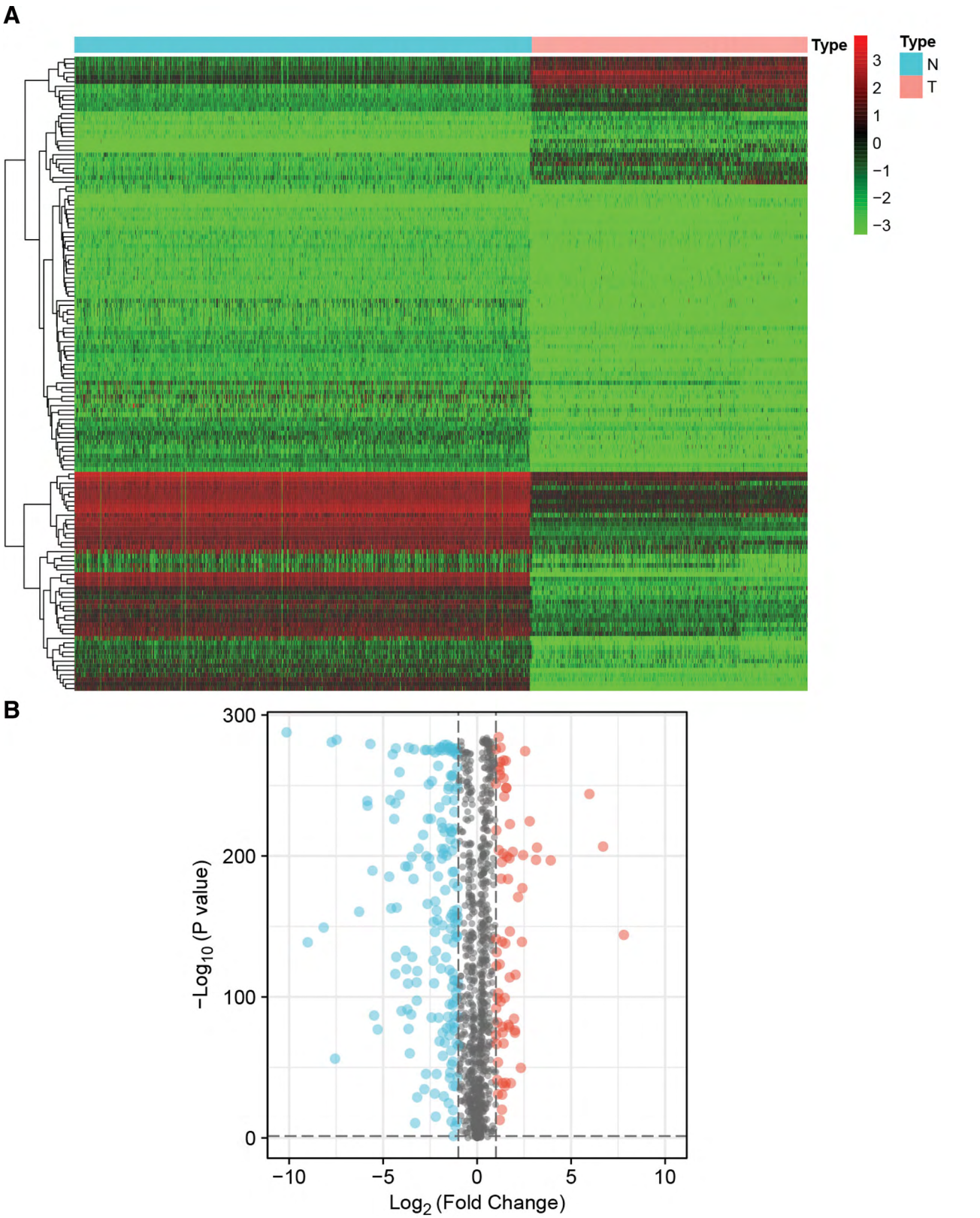

Figure 2. Identification of the DEGs. Lipid metabolism-related DEGs were screened (tumor vs normal) in TCGA dataset and visualized with a heatmap (A) and volcano plot (B). DEGs = differentially expressed genes, TCGA = the Cancer Genome Atlas.

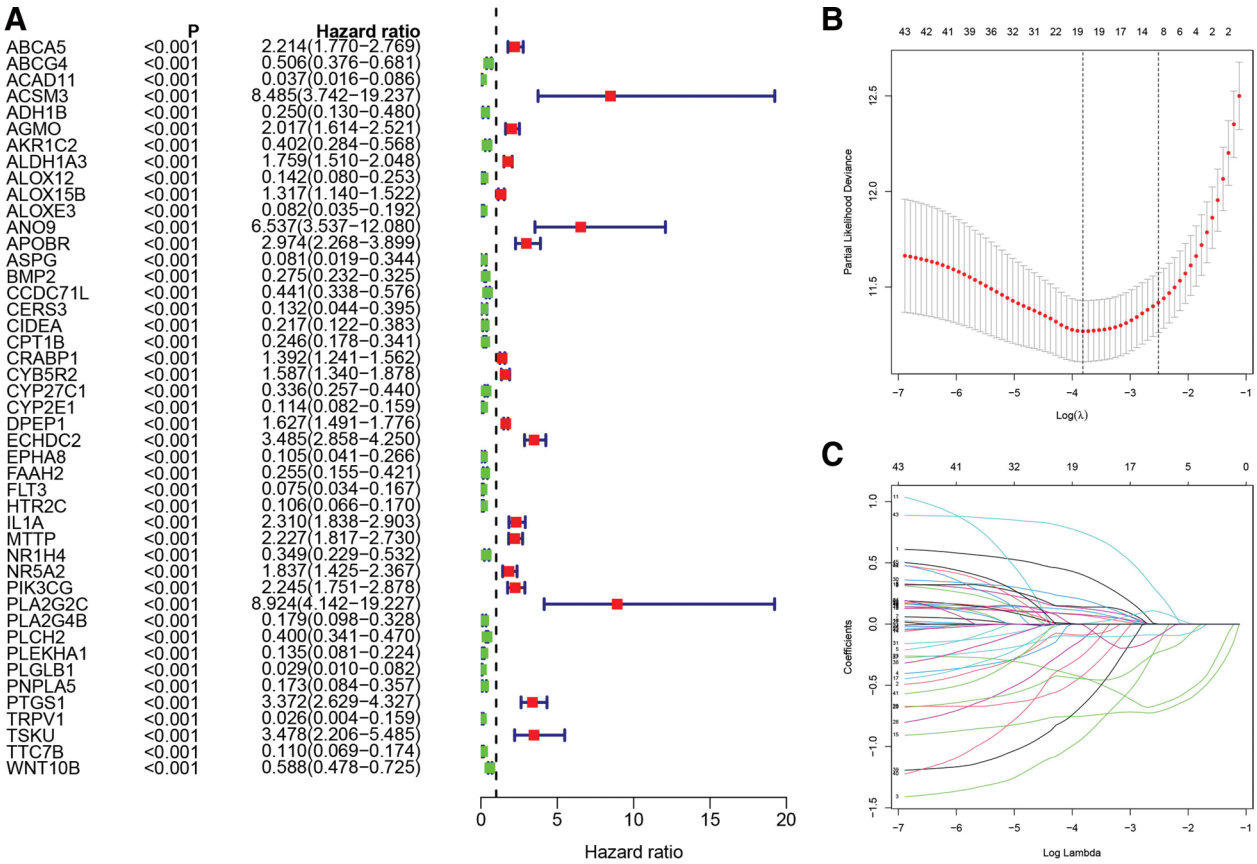

Figure 3. Establishment of the risk score. Based on the univariate Cox analysis, DEGs were significantly associated with the prognosis of patients with gliomas ($P < .001$) (A). The selected genes were included in the LASSO Cox regression model (B), and the risk score was calculated from the coefficients for each gene (C). DEGs = differentially expressed genes, LASSO = least absolute shrinkage and selection operator.

Table 3

The coefficients of included genes.

ID	Gene name	Coefficients
ABCA5	ATP binding cassette subfamily A member 5	0.04447
ABCG4	ATP binding cassette subfamily G member 4	0.01257
ACAD11	acyl-CoA dehydrogenase family member 11	0.00087
AGMO	alkylglycerol monooxygenase	−0.00007
ALDH1A3	aldehyde dehydrogenase 1 family member A3	−0.00171
ALOX15B	arachidonate 15-lipoxygenase type B	0.00287
APOBR	apolipoprotein B	−0.21707
BMP2	bone morphogenetic protein 2	0.01956
CRABP1	cellular retinoic acid binding protein 1	−0.01630
CYP2E1	cytochrome P450 family 2 subfamily E member 1	−0.01290
ECHDC2	enoyl-CoA hydratase domain containing 2	−0.02504
EPHA8	EPH receptor A8	0.00371
FLT3	fms related receptor tyrosine kinase 3	−0.00607
HTR2C	5-hydroxytryptamine receptor 2C	0.01463
IL1A	interleukin 1 alpha	−0.00072
PLCH2	phospholipase C eta 2	0.12151
PLGLB1	plasminogen like B1	−0.73505
PNPLA5	patatin like phospholipase domain containing 5	0.04197
TSKU	tsukushi, small leucine rich proteoglycan	0.13857
TTC7B	tetratricopeptide repeat domain 7B	−0.32989

C) (Table 3). The high-risk and low-risk groups were distinguished by the median risk score (Fig. 4A and B). The areas under the curves at 1 year, 3 years and 5 years were 0.867, 0.910, and 0.879, respectively (Fig. 4C). The high-risk group had a significantly lower survival rate than the low-risk group ($P < .001$) (Fig. 4D). The risk score was then validated using the CGGA dataset (Fig. 4E and F). The areas under the curves at 1-year, 3-year, and 5-year were 0.753, 0.762, and 0.747, respectively (Fig. 4G). The high-risk group also had a significantly lower survival rate than the low-risk group ($P < .001$) (Fig. 4H).

The results of both univariate and multivariate Cox regression analyses indicated that the risk score independently predicted the prognosis of patients with gliomas patients in TCGA dataset (Fig. 5A and B), and the results from the analysis of the risk score using the CGGA dataset were consistent with those obtained using TCGA dataset (Fig. 5C and D). The nomogram and calibration curves constructed based on the risk score predicted 1-year, 3-year, and 5-year overall survival of patients in both TCGA (Fig. 6A–D) and CGGA datasets (Fig. 7A–D).

The results of immunohistochemical staining for the proteins encoded by the 20 genes included in the risk signature showed that the expression patterns of 9 genes were consistent with our previous DEG analysis (ABCA5, ACAD11, APOBR, CYP2E1, EPH48, PLCH2, PNPLA5, TSKU, and TTC7B) (Fig. 8A–R). Of the remaining 11 genes, the immunohistochemical images of 6 genes were not included in the Human Protein Atlas database (AGMO, BMP2, FLT3, HTR2C, IL1A, and PLGLB1), 4 genes were not detected in the immunohistochemical images of tumor tissues and normal tissues (ABCG4, ALOX15B, CRABP1, and ECHDC2), and the expression trend of 1 gene was opposite to that found in our study (ALDH1A3).

3.2. Immune-related parameters and the risk score

According to the ESTIMATE algorithm, the risk score based on TCGA dataset was significantly positively correlated with the stromal score and immune score and was significantly negatively correlated with tumor purity (all P values <.001) (Fig. 9A–C). The results from the CGGA dataset were consistent with those from TCGA dataset (Fig. 9D–F).

The differences in the expression of common immune checkpoint genes in the 2 risk groups were explored, and the results indicated that the expression of common immune checkpoint genes in the high-risk group were upregulated in both TCGA (Fig. 10A) and CGGA datasets (Fig. 10B). Differences in immune cells in the 2 risk groups were assessed using the CIBERSORT algorithm. In TCGA dataset, increased infiltration levels of memory B cells, CD8 T cells, activated memory CD4 T cells, regulatory T cells (Tregs), gamma delta T cells, resting mast cells, resting memory CD4 T cells, follicular helper T cells, M0 macrophages, M1 macrophages and neutrophil were observed in the high-risk group. Increased infiltration levels of eosinophils, CD4 naive T cells, monocytes and mast cell-activated were observed in the low-risk group (Fig. 10C). The CGGA results were mostly consistent with TCGA results (Fig. 10D).

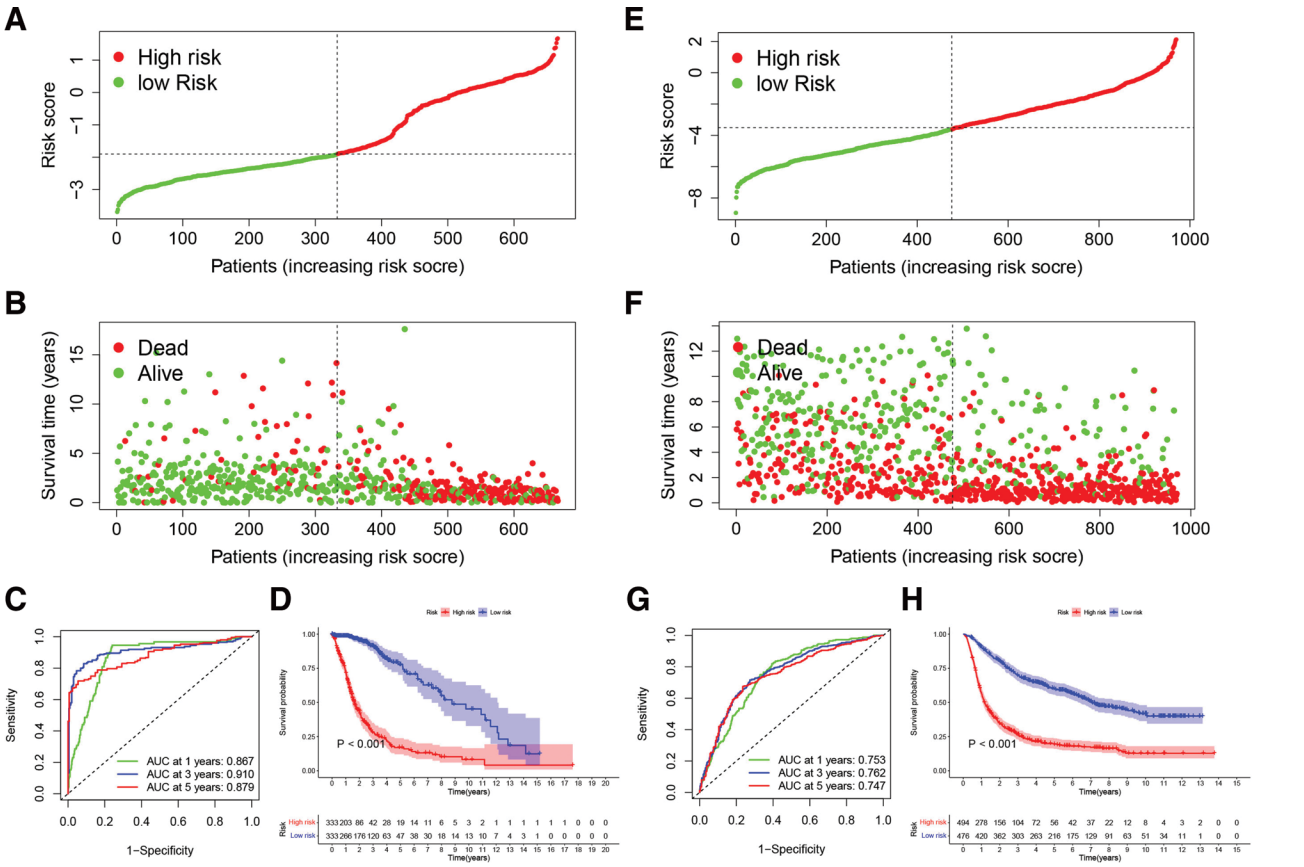

Figure 4. The risk signature. Patients with gliomas in TCGA dataset were distributed into different risk groups (A). Survival status of patients with gliomas in different risk groups (B). The AUCs of the ROC curves at 1 year, 3 years and 5 years were 0.867, 0.910, and 0.879, respectively (C). The high-risk group had a significantly lower survival rate than the low-risk group (D). Patients with gliomas in the CGGA dataset were distributed into different risk groups (E). Survival status of patients with gliomas in different risk groups (F). The AUCs of the ROC curves at 1 year, 3 years and 5 years were 0.867, 0.910, and 0.879, respectively (G). The high-risk group had a significantly lower survival rate than the low-risk group (H). AUC = area under the curve, CGGA = Chinese gliomas genome atlas, ROC = receiver operating characteristic, TCGA = The Cancer Genome Atlas.

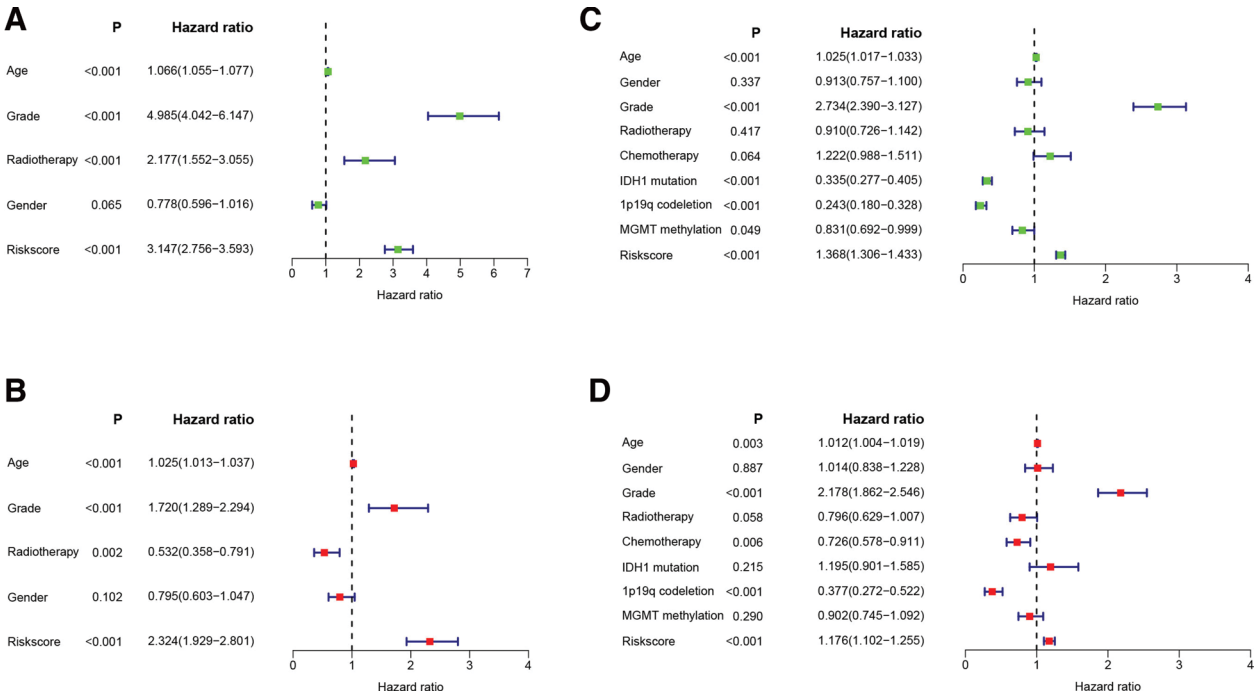

Figure 5. Independent prognostic analysis of the risk score. In TCGA dataset, the results of both univariate and multivariate Cox regression analyses indicated that the risk score independently predicted the prognosis of patients with gliomas (A and B), and the results from the analysis of the risk score of patients in the CGGA dataset were consistent with those from TCGA (C and D). CGGA = Chinese gliomas genome atlas, IDH1 = isocitrate dehydrogenase 1, MGMT = O6-methylguanine-DNA methyl-transferase, TCGA = The Cancer Genome Atlas.

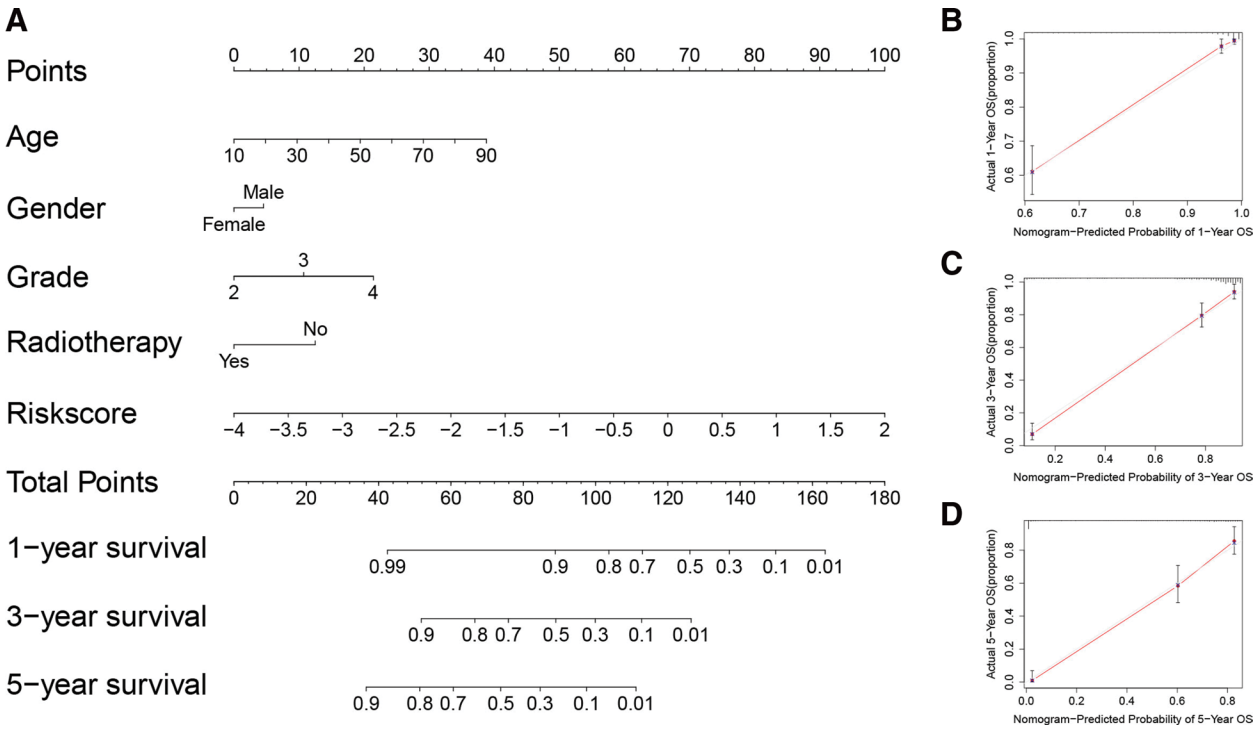

Figure 6. Construction of a nomogram with TCGA dataset. Nomograms (A) and calibration curves (B–D) constructed based on the risk score predicted 1-year, 3-year, and 5-year OS of patients in TCGA dataset. OS = overall survival, TCGA = The Cancer Genome Atlas.

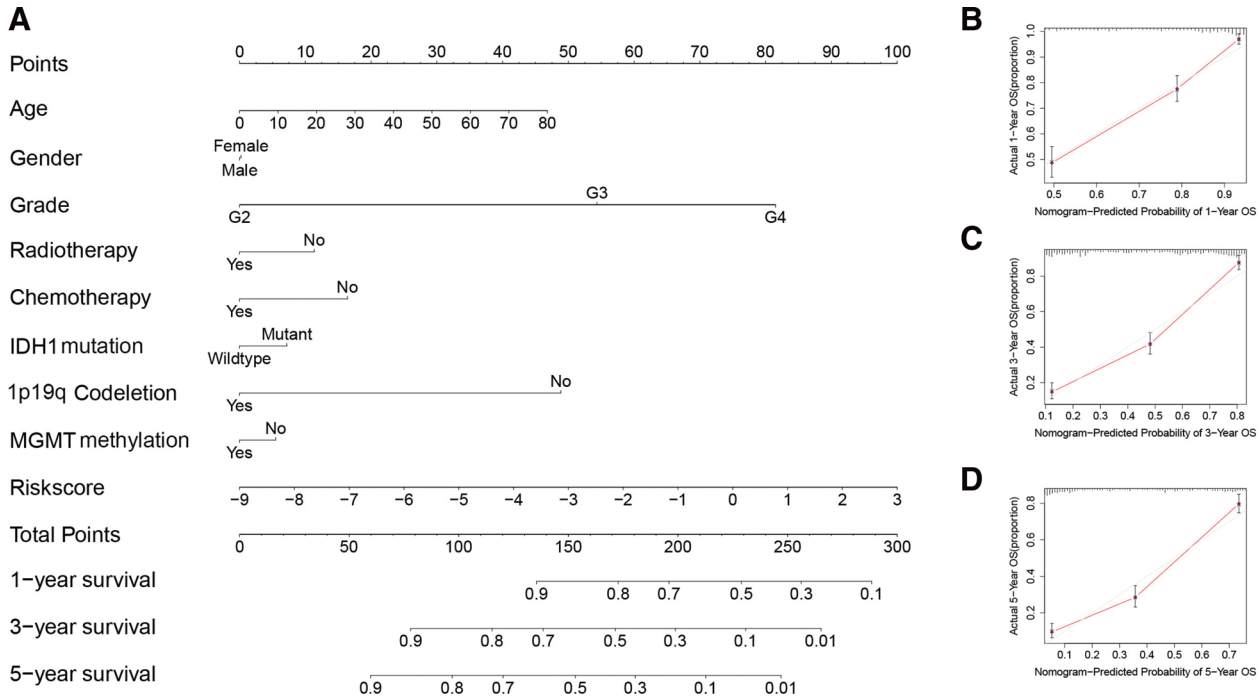

Figure 7. Construction of a nomogram with the CGGA dataset. Nomograms (A) and calibration curves (B–D) constructed based on the risk score predicted 1-year, 3-year, and 5-year OS of patients in the CGGA dataset. CGGA = Chinese gliomas genome atlas, IDH1 = isocitrate dehydrogenase 1, MGMT = O6-methylguanine-DNA methyltransferase, OS = overall survival.

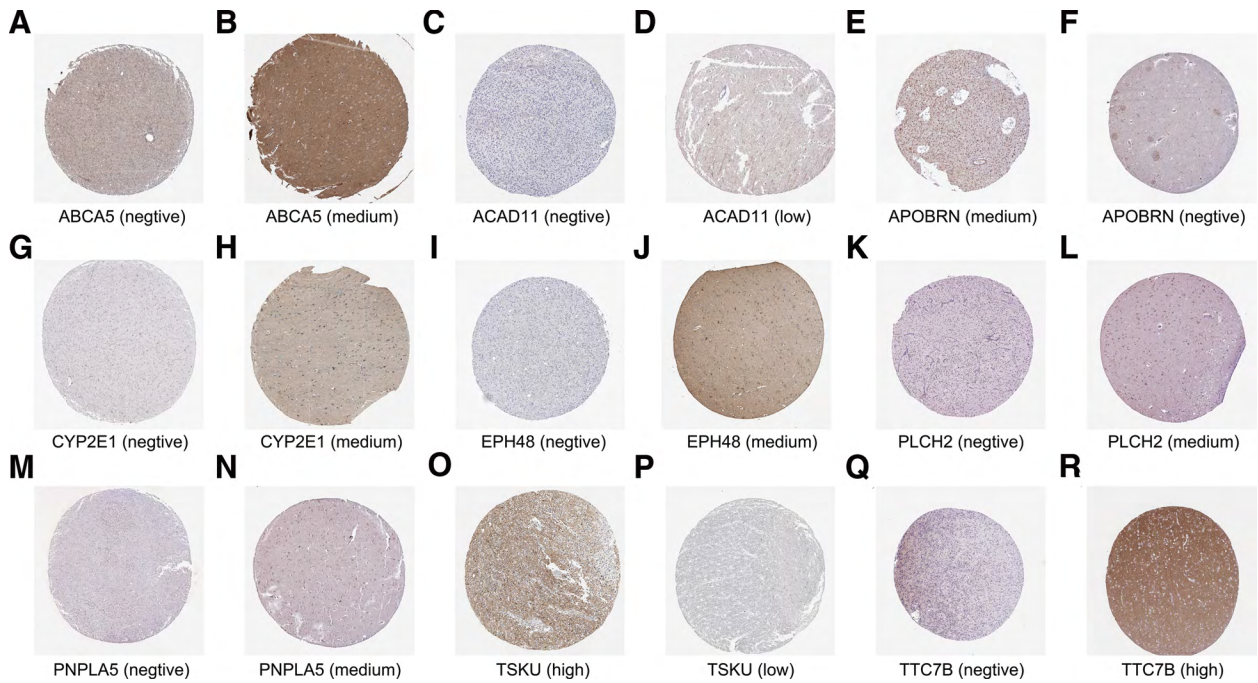

Figure 8. Validation of the expression of genes selected to constitute the risk signature according to the HPA database. Images of immunohistochemical staining for the proteins encoded by the 20 genes selected to constitute the risk signature showed that the expression patterns of 9 genes were consistent with our previous DEG analysis (A–R). HPA = human protein atlas.

3.3. PPI network and coexpression analysis

A PPI network was constructed, and coexpression analysis was performed based on the genes included in the risk signature. CYP2E1 formed the most connections with other genes in the PPI network (Fig. 11A) and had significant coexpression relationships with other genes (Fig. 11B); thus, CYP2E1 was regarded as a hub gene. The relationships between CYP2E1 and various clinical parameters were then explored. In TCGA dataset, CYP2E1 expression was increased in normal tissues (Fig. 12A), younger patients (Fig. 12B), those who did not receive radiotherapy (Fig. 12C) and patients with LGGs (Fig. 12D); its expression was also not related to gender (Fig. 12E). High expression indicated a better clinical

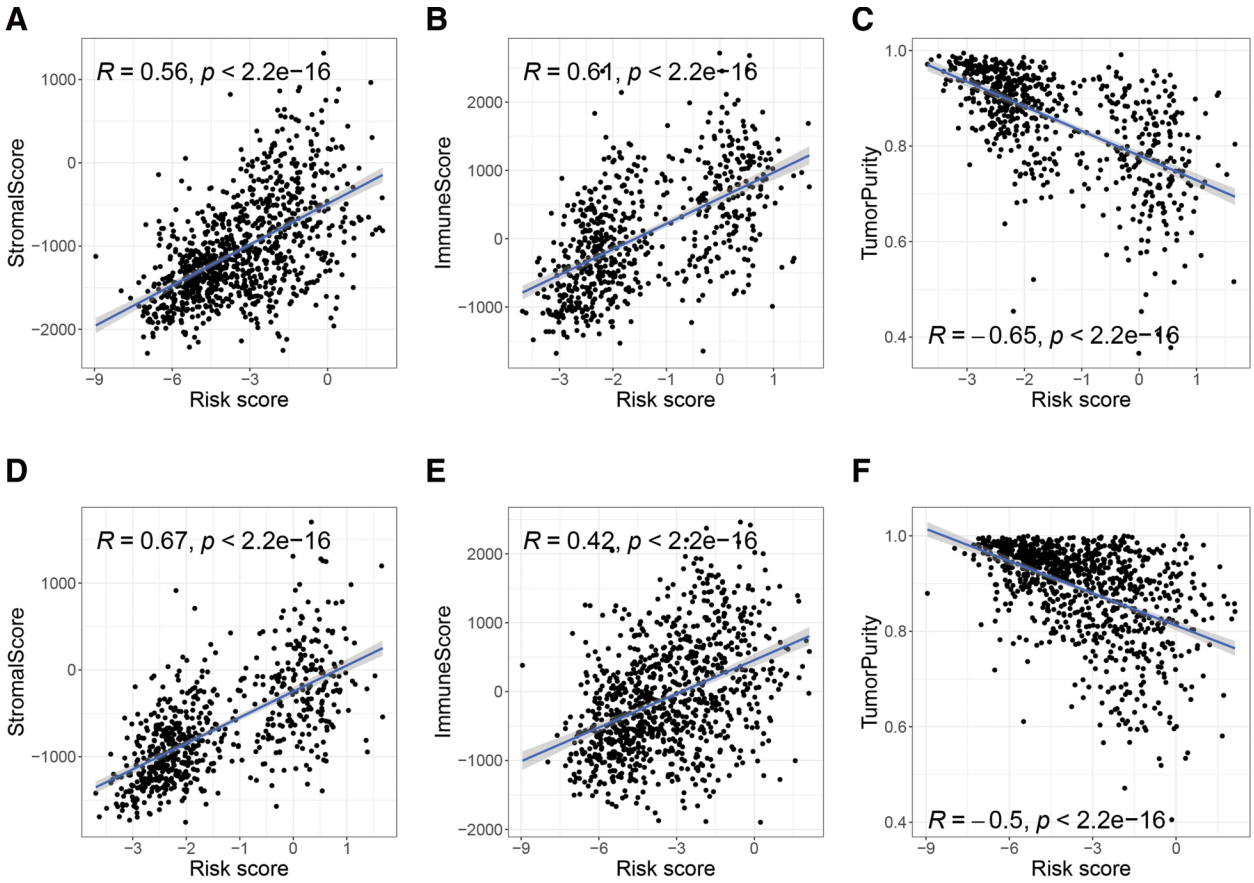

Figure 9. Risk score and TME. According to the ESTIMATE algorithm, the risk score in TCGA dataset was significantly positively correlated with the stromal score (A) and immune score (B) and was significantly negatively correlated with tumor purity (C). The results from the CGGA dataset were consistent with those from TCGA dataset (D-F). CGGA = Chinese gliomas genome atlas, ESTIMATE = estimation of stromal and immune cells in malignant tumor tissues using expression data, TCGA = The Cancer Genome Atlas, TME = tumor microenvironment.

outcome (Fig. 12F). In the CGGA dataset, CYP2E1 expression was increased in patients who were younger (Fig. 12G), those who did not undergo chemotherapy (Fig. 12H), and those who had LGGs (Fig. 12I), isocitrate dehydrogenase 1 mutation (Fig. 12J), 1p19q codeletion (Fig. 12K) and O6-methylguanine-DNA methyl-transferase methylation (Fig. 12L). Its expression was not related to the radiotherapy status (Fig. 12M) or gender (Fig. 12N). High expression also indicated a better clinical outcome (Fig. 12O).

3.4. Risk score and drug sensitivity

The results of the drug sensitivity analysis showed that 6 common chemotherapy drugs had higher half-maximal inhibitory concentration (IC50) levels in the low-risk group in both TCGA (Fig. 13A–F) and CGGA datasets (Fig. 13G–L), suggesting that the high-risk group was more sensitive to chemotherapy drugs. In addition, the TMB was significantly positively correlated with the risk score (Fig. 14A), indicating that ICIs exerted a better treatment effect on the high-risk group, which was consistent with the results from the TIDE database (Fig. 14B).

3.5. Biological functions and pathways

The results for gene set enrichment in the high-risk and low-risk groups of patients obtained using the gene ontology analysis are shown in Tables 4 and 5, respectively. The results for gene set enrichment in the high-risk patients obtained using the Kyoto encyclopedia of genes and genomes (KEGG) analysis are shown in Table 6. No gene sets were significantly enriched in low-risk patients in the KEGG analysis.

4. Discussion

The connections among metabolism, immunity and cancer deserve further exploration. Dysregulated metabolic processes, such as glucose metabolism,[25] protein metabolism,[26] and lipid metabolism,[26] lead to tumor development and immune cell dysfunction. Lipid metabolism in tumors, the focus of our study, has been shown to be involved in both cellular signaling and the energy supply.[8] Dysregulation of lipid metabolism and related enzymes in gliomas has been reported.[27–29] Therefore, lipid metabolism represents a new research direction in the field of cancer therapy. Compared with previous studies,[30–32] the research contents of our study were relatively more comprehensive. Our focus was only on lipid metabolism, not all metabolic processes, which might reduce the number of confounding factors and explain the significant role of lipid metabolism in gliomas, thus providing a new perspective for the treatment of gliomas. Furthermore, compared with other metabolic processes, the roles of lipid metabolism in gliomas have been less extensively studied and deserve further analysis.

In our study, a risk signature containing 20 genes was constructed based on DEGs related to lipid metabolism in gliomas. Patients with gliomas in the high-risk group had a poor prognosis, and the risk score was associated with multiple immunological parameters, sensitivity to common chemotherapy drugs, and biological functions. In addition, a hub gene in the risk signature, CYP2E1, was identified by the coexpression analysis and was present in the constructed PPI network. CYP2E1, a member of the cytochrome 450 family, promotes lipid production by inducing oxidative stress and is differentially expressed in a

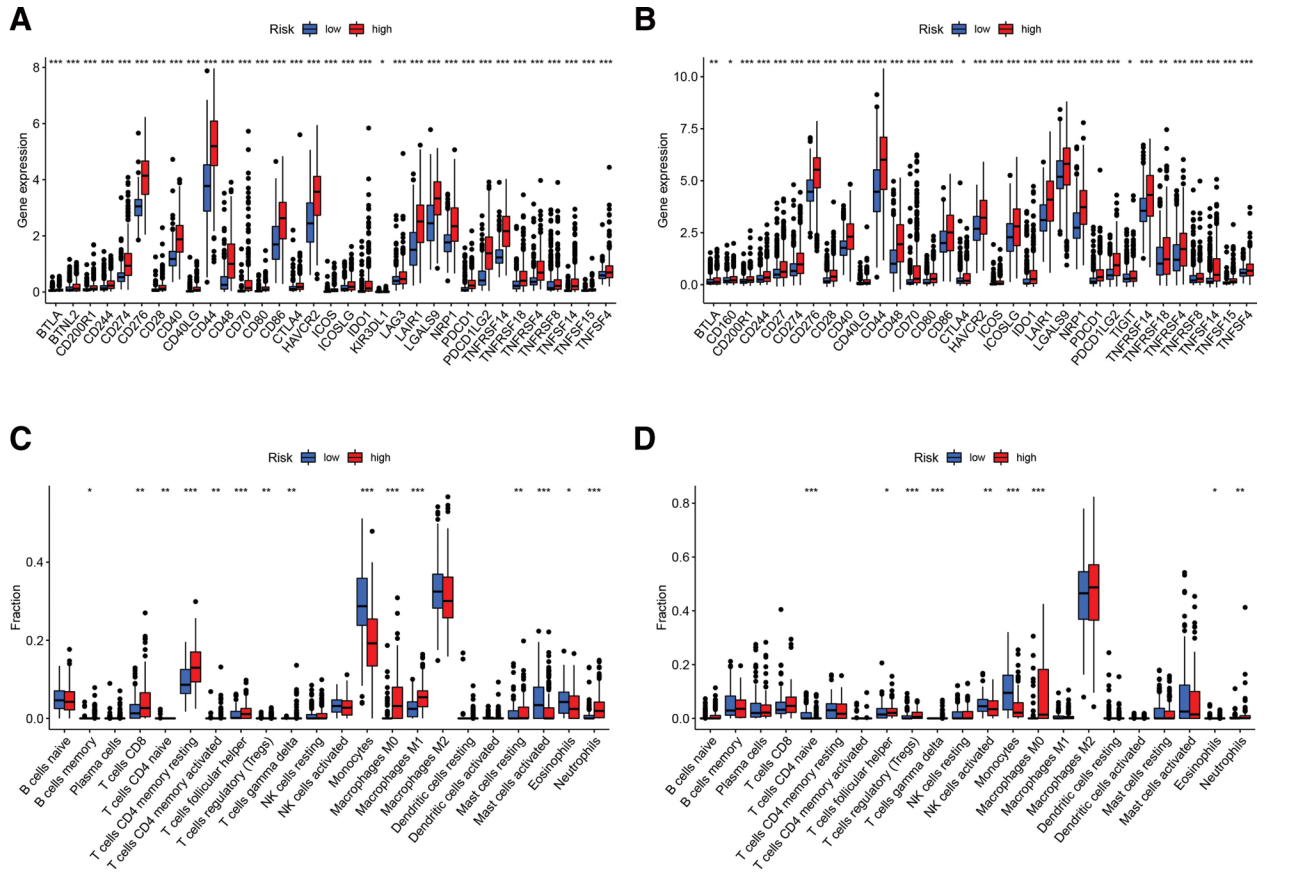

Figure 10. Analysis of immune checkpoint expression and immune cell infiltration between the 2 risk groups. The expression of common immune checkpoints in the high-risk group was upregulated in both TCGA and CGGA datasets (A and B). Differences in immune cell infiltration between the 2 risk groups were assessed using the CIBERSORT algorithm. In TCGA dataset, increased levels of memory B cells, CD8 T cells, activated memory CD4 T cells, regulatory T cells, gamma delta T cells, resting mast cells, resting memory CD4 T cells, follicular helper T cells, M0 macrophages, M1 macrophages and neutrophil infiltration were observed in the high-risk group. Increased levels of eosinophils, naive CD4 T cells, monocytes and mast cell-activated infiltration were observed in the low-risk group (C). The results from the CGGA dataset were mostly consistent with the results from TCGA dataset (D). CGGA = Chinese gliomas genome atlas, CIBERSORT = estimating relative subsets of RNA transcripts, mRNA = messenger RNA, TCGA = the Cancer Genome Atlas.

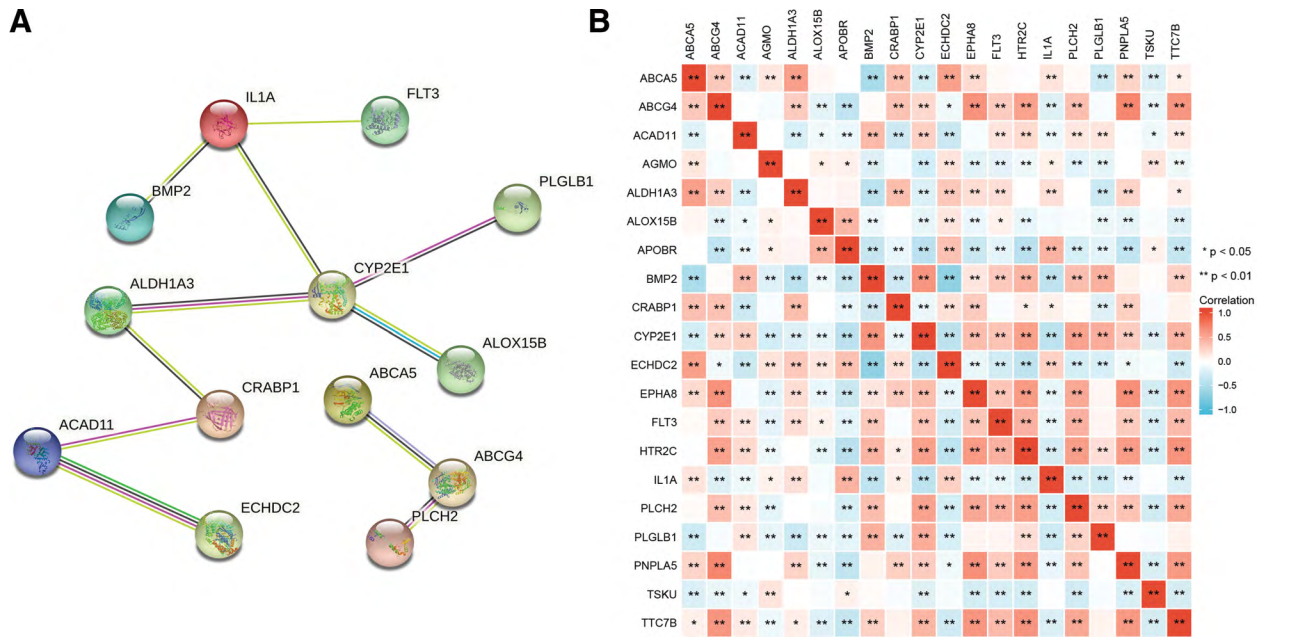

Figure 11. PPI network and coexpression analysis. By constructing a PPI network (A) and performing a coexpression analysis (B) based on the genes included in the risk signature, the results showed that CYP2E1 formed the most connections with other genes in the PPI network and exhibited significant coexpression relationships with other genes; therefore, CYP2E1 was identified as a hub gene. PPI = protein–protein interaction.

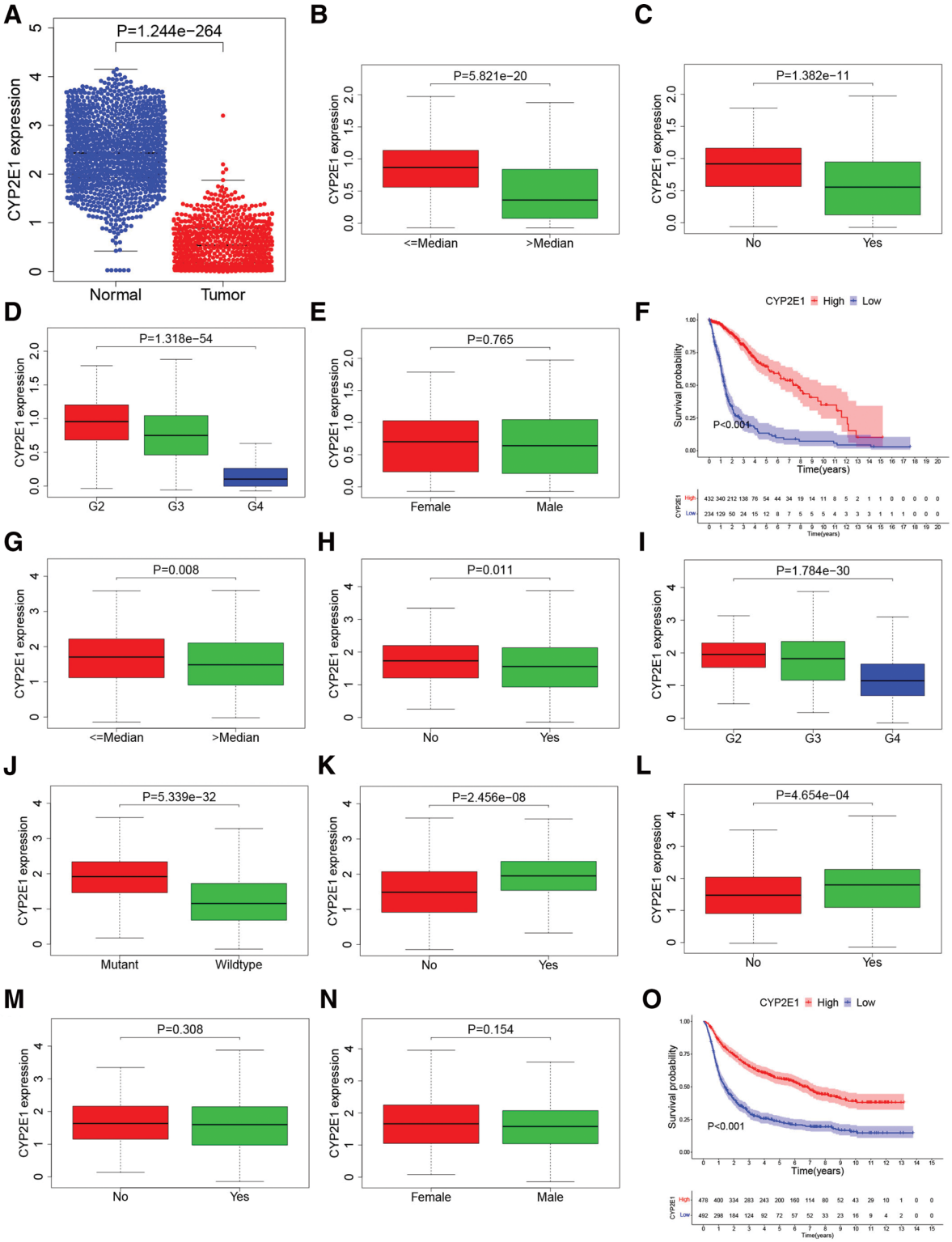

Figure 12. CYP2E1 and numerous clinical features. In TCGA dataset, the results suggested that CYP2E1 expression was increased in normal tissues (A), younger patients (B), patients who did not receive radiotherapy (C) and patients with low-grade gliomas (D), and its expression was not related to gender (E). High expression indicated a better clinical outcome (F). In the CGGA dataset, the results suggested that CYP2E1 expression was increased in patients who were younger (G), those who did not receive chemotherapy (H), and those who had low-grade gliomas (I), IDH1 mutation (J), 1p19q codeletion (K) and MGMT methylation (L), and its expression was not related to the radiotherapy status (M) or gender (N). High expression also indicated a better clinical outcome (O). CGGA = Chinese gliomas genome atlas, IDH1 = isocitrate dehydrogenase 1, MGMT = O6-methylguanine-DNA methyltransferase, TCGA = The Cancer Genome Atlas.

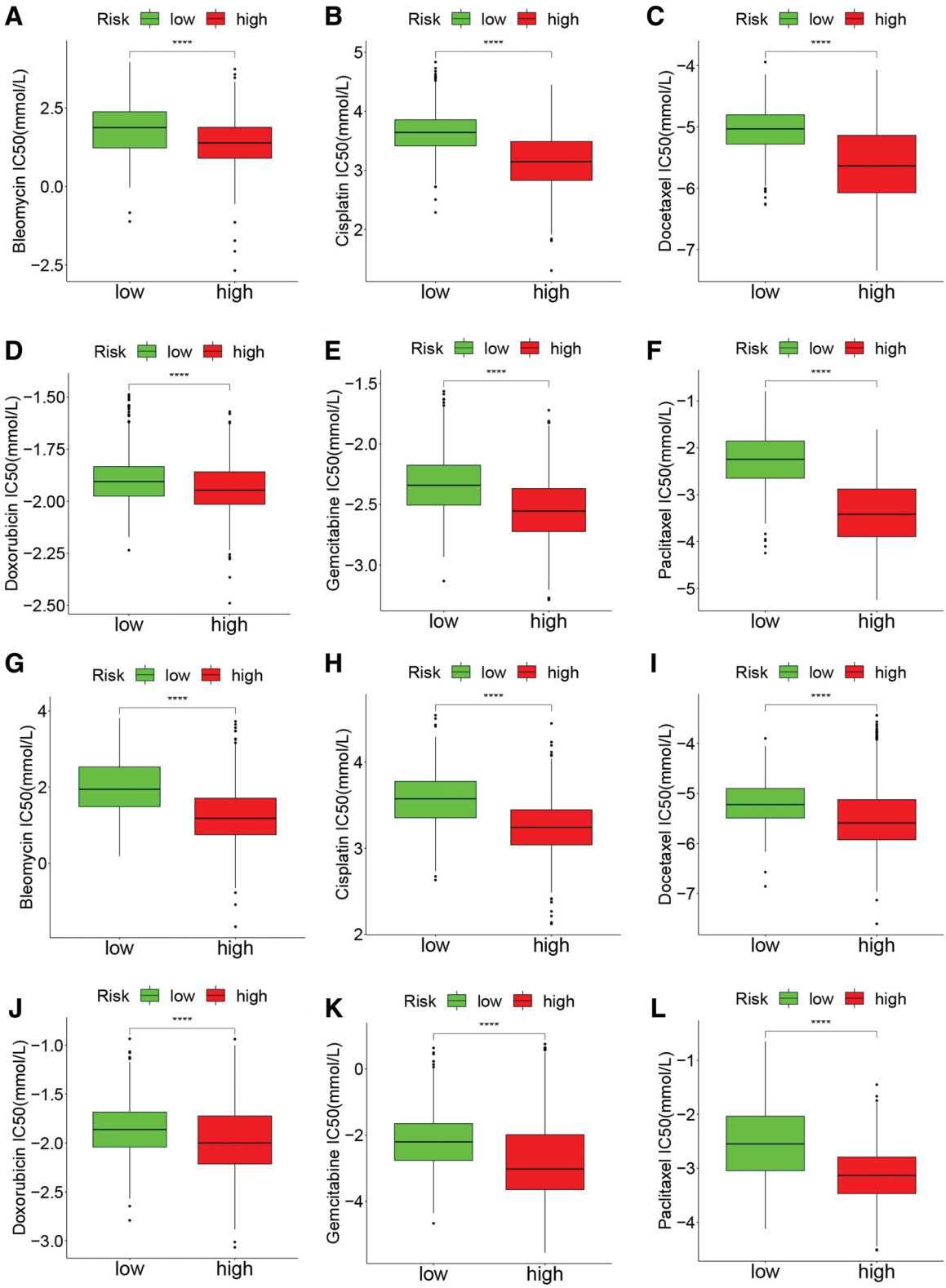

Figure 13. Risk score and drug sensitivity. The results of the drug sensitivity analysis showed that 6 common chemotherapy drugs (bleomycin, cisplatin, docetaxel, doxorubicin, gemcitabine, and paclitaxel) had higher IC50 levels in the low-risk group in both TCGA (A–F) and CGGA datasets (G–L), suggesting that the high-risk group was more sensitive to chemotherapy drugs. CGGA = Chinese gliomas genome atlas, IC50 = half-maximal inhibitory concentration, TCGA = The Cancer Genome Atlas.

variety of tumors; it has also been reported to affect antitumor drug metabolism.[33–36] A previous study confirmed that CYP2E1 acts as a tumor suppressor in gliomas, consistent with our findings, suggesting that this hub gene could be a key target for follow-up studies.[37]

The correlation analysis revealed that the risk score may be significantly correlated with various immunology-related parameters. Elevated expression of immune checkpoint proteins that facilitate immune escape was observed in high-risk patients with gliomas, and thus the microenvironment of high-risk patients

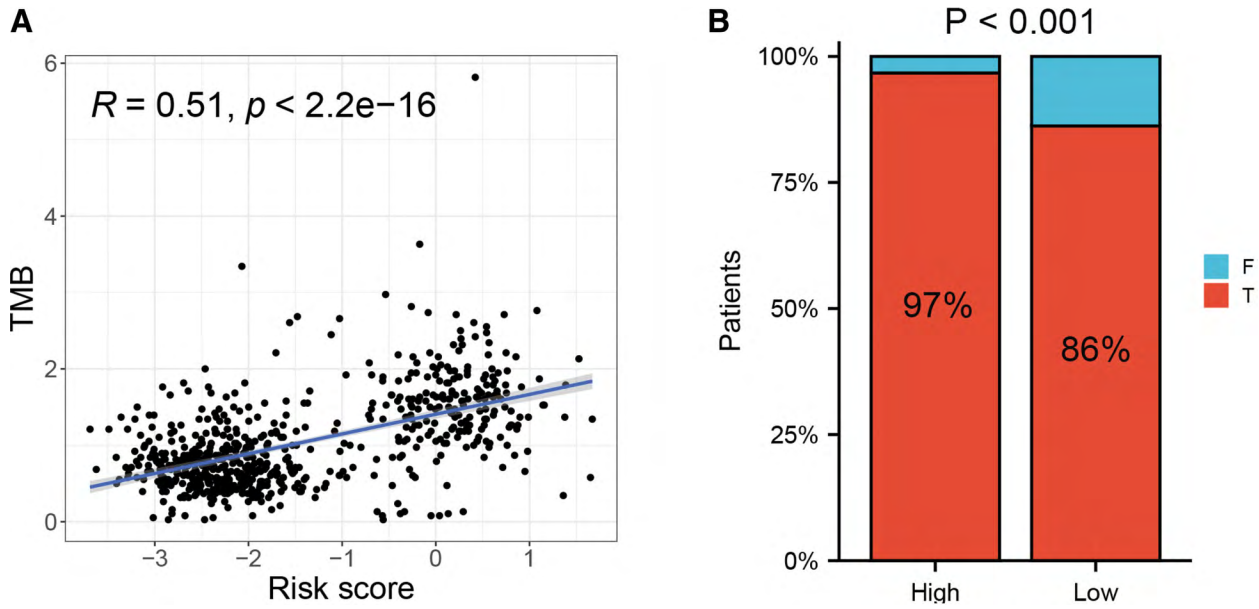

Figure 14. Risk score and ICIs. TMB was significantly positively correlated with the risk score (A), suggesting that the high-risk group experienced a better ICI treatment effect, consistent with the results from the TIDE database (B). ICIs = immune checkpoint inhibitors, TMB = tumor mutational burden.

Table 4

Gene sets enriched in the high-risk phenotype via GO.

Gene set name	NES	NOM *P* value	FDR *Q* value
GOMF_EXTRACELLULAR_MATRIX_STRUCTURAL_CONSTITUENT	1.903	.002	0.142
GOMF_COLLAGEN_BINDING	1.876	.000	0.149
GOBP_POSITIVE_REGULATION_OF_CELL_CELL_ADHESION	1.851	.004	0.129
GOCC_COLLAGEN_CONTAINING_EXTRACELLULAR_MATRIX	1.834	.004	0.120
GOBP_NEGATIVE_REGULATION_OF_IMMUNE_RESPONSE	1.828	.015	0.120
GOBP_NEGATIVE_REGULATION_OF_IMMUNE_SYSTEM_PROCESS	1.827	.013	0.118
GOBP_POSITIVE_REGULATION_OF_FIBROBLAST_PROLIFERATION	1.819	.004	0.111
GOBP_SMOOTH_MUSCLE_CELL_MIGRATION	1.812	.004	0.104
GOBP_REGULATION_OF_COLLAGEN_METABOLIC_PROCESS	1.805	.008	0.101
GOBP_FIBROBLAST_PROLIFERATION	1.781	.000	0.097
GOBP_POSITIVE_REGULATION_OF_ENDOTHELIAL_CELL_CHEMOTAXIS	1.701	.006	0.097
GOBP_POSITIVE_REGULATION_OF_SMOOTH_MUSCLE_CELL_MIGRATION	1.684	.013	0.099
GOBP_REGULATION_OF_ENDOTHELIAL_CELL_CHEMOTAXIS	1.664	.016	0.100
GOBP_OSTEOBLAST_DIFFERENTIATION	1.647	.009	0.102
GOBP_POSITIVE_REGULATION_OF_EPITHELIAL_TO_MESENCHYMAL_TRANSITION	1.639	.035	0.104
GOBP_POSITIVE_REGULATION_OF_COLLAGEN_METABOLIC_PROCESS	1.617	.038	0.111
GOBP_POSITIVE_REGULATION_OF_OSTEOBLAST_DIFFERENTIATION	1.608	.029	0.113
GOBP_POSITIVE_REGULATION_OF_FATTY_ACID_METABOLIC_PROCESS	1.516	.041	0.144
GOBP_REGULATION_OF_FATTY_ACID_METABOLIC_PROCESS	1.442	.043	0.178
GOBP_GLUCOSE_METABOLIC_PROCESS	1.428	.037	0.183

Gene sets with NOM *P* value <.05 and FDR *Q* value <0.25 were considered significant.
FDR = false discovery rate, GO = gene ontology, NES = normalized enrichment score, NOM = nominal.

with gliomas could be characterized as immunosuppressive.[38] The results from the ESTIMATE algorithm suggested that patients in high-risk group had higher level of stromal cell infiltration, higher level of immune cell infiltration, and lower tumor purity, which appeared to contradict the immune checkpoint analysis. However, the results from the CIBERSORT algorithm showed that the immune cells that were significantly enriched in high-risk patients in both TCGA and CGGA datasets were regulatory T cells (Tregs), gamma delta T cells, follicular helper T cells, M0 macrophages, and neutrophils. The immune cells that were significantly enriched in low-risk patients in both TCGA and CGGA datasets were CD4 naive T cells and monocytes. Although the high-risk group showed enrichment of more types of immune cells than the low-risk group, Treg cells and M0 macrophages have been reported to play an immunosuppressive role in gliomas, and Treg cells, neutrophils and M0 macrophages are associated with the malignant clinical features of gliomas, indicating the predominance of cancer-promoting immune cells

Table 5

Gene sets enriched in the low-risk phenotype via GO.

Gene set name	NES	NOM *P* value	FDR *Q* value
GOMF_UBIQUITIN_LIKE_PROTEIN_SPECIFIC_PROTEASE_ACTIVITY	−1.947	.000	0.249
GOBP_PEPTIDYL_LYSINE_TRIMETHYLATION	−1.945	.000	0.236
GOBP_ESTABLISHMENT_OF_PROTEIN_LOCALIZATION_TO_VACUOLE	−1.943	.000	0.227
GOBP_N_TERMINAL_PROTEIN_AMINO_ACID_MODIFICATION	−1.942	.000	0.214
GOBP_NEUROMUSCULAR_PROCESS_CONTROLLING_BALANCE	−1.935	.000	0.217
GOBP_REGULATION_OF_MRNA_PROCESSING	−1.925	.006	0.227
GOBP_PROTEIN_ACYLATION	−1.925	.000	0.216
GOBP_LIGAND_GATED_ION_CHANNEL_SIGNALING_PATHWAY	−1.924	.000	0.206
GOCC_PROTEIN_ACETYLTRANSFERASE_COMPLEX	−1.921	.010	0.202
GOBP_ENDOSOMAL_TRANSPORT	−1.911	.004	0.217
GOBP_POSITIVE_REGULATION_OF_MRNA_SPLICING_VIA_SPLICEOSOME	−1.909	.002	0.210
GOCC_MAGNESIUM_DEPENDENT_PROTEIN_SERINE_THREONINE_PHOSPHATASE_COMPLEX	−1.905	.004	0.209
GOBP_REGULATION_OF_MRNA_POLYADENYLATION	−1.903	.000	0.205
GOBP_REGULATION_OF_MRNA_SPLICING_VIA_SPLICEOSOME	−1.900	.008	0.202
GOBP_LYSOSOMAL_TRANSPORT	−1.896	.004	0.204
GOBP_CYTOPLASMIC_MICROTUBULE_ORGANIZATION	−1.895	.006	0.197
GOBP_L_GLUTAMATE_TRANSMEMBRANE_TRANSPORT	−1.895	.004	0.190
GOBP_RESPONSE_TO_POTASSIUM_ION	−1.894	.000	0.187
GOBP_REGULATION_OF_TRANSCRIPTION_ELONGATION_FROM_RNA_POLYMERASE_II_PROMOTER	−1.892	.004	0.183
GOBP_STARTLE_RESPONSE	−1.892	.000	0.178

Gene sets with NOM *P* value <.05 and FDR *Q* value <0.25 were considered significant.

FDR = false discovery rate, GO = gene ontology, mRNA = messenger RNA, NES = normalized enrichment score, NOM = nominal.

Table 6

Gene sets enriched in the high-risk phenotype via KEGG.

Gene set name	NES	NOM *P* value	FDR *Q* value
KEGG_GLUTATHIONE_METABOLISM	2.034	.000	0.052
KEGG_AMINO_SUGAR_AND_NUCLEOTIDE_SUGAR_METABOLISM	1.967	.000	0.067
KEGG_ECM_RECEPTOR_INTERACTION	1.863	.010	0.117
KEGG_PANTOTHENATE_AND_COA_BIOSYNTHESIS	1.791	.010	0.106
KEGG_LEUKOCYTE_TRANSENDOTHELIAL_MIGRATION	1.779	.019	0.106
KEGG_INTESTINAL_IMMUNE_NETWORK_FOR_IGA_PRODUCTION	1.775	.010	0.100
KEGG_PYRIMIDINE_METABOLISM	1.771	.014	0.096
KEGG_CELL_CYCLE	1.768	.033	0.091
KEGG_CYTOKINE_CYTOKINE_RECEPTOR_INTERACTION	1.753	.014	0.080
KEGG_FOCAL_ADHESION	1.737	.025	0.077
KEGG_TOLL_LIKE_RECEPTOR_SIGNALING_PATHWAY	1.709	.026	0.078
KEGG_ANTIGEN_PROCESSING_AND_PRESENTATION	1.685	.034	0.082
KEGG_PRIMARY_IMMUNODEFICIENCY	1.684	.033	0.080
KEGG_JAK_STAT_SIGNALING_PATHWAY	1.676	.019	0.081
KEGG_DNA_REPLICATION	1.651	.028	0.085
KEGG_GALACTOSE_METABOLISM	1.643	.020	0.087
KEGG_NICOTINATE_AND_NICOTINAMIDE_METABOLISM	1.583	.032	0.097
KEGG_TYROSINE_METABOLISM	1.545	.032	0.112
KEGG_RIG_I_LIKE_RECEPTOR_SIGNALING_PATHWAY	1.541	.043	0.112

Gene sets with NOM *P* value <.05 and FDR *Q* value <0.25 were considered significant.

FDR = false discovery rate, KEGG = Kyoto encyclopedia of genes and genomes, NES = normalized enrichment score, NOM = nominal.

in the high-risk group.[39–42] The monocytes that were enriched in the low-risk group were antigen-presenting cells that elicited significant antitumor effects.[43] Interestingly, the levels of infiltrating CD8 + and CD4 + T cells in high-risk patients with gliomas were higher than those in low-risk patients. We hypothesized that the constant exposure of neoantigens due to the strong malignant proliferation ability of gliomas in the high-risk group would activate the immune response and increase the

infiltration of CD4+ and CD8+ T cells in the high-risk group. However, if T cells were continuously exposed to neoantigens, T cell exhaustion could occur, which was manifested by the loss of T cell functions and an increase in the expression of various immunosuppressive factors, resulting in immunosuppression in the tumor microenvironment and finally promoting tumor progression.[44,45] In addition, the increased number of stromal cells observed in the high-risk group might mediate immune escape, rendering these patients resistant to immunotherapy.[46] Therefore, the comprehensive analysis has shown that the poor prognosis of patients with gliomas in the high-risk group is due to immunosuppression caused by multiple factors.

Gliomas are resistant to chemotherapy due to their high heterogeneity and increased proliferation rate.[47,48] According to the results of the drug sensitivity analysis, patients in the high-risk group were more sensitive to 6 common chemotherapy drugs. Differences in the TMB and the effects of ICI treatment between the 2 risk groups were further evaluated. The TMB is considered a biomarker for the response to ICI treatment, and a higher TMB implies better ICI efficacy.[49] In our study, the results from the TIDE database showed that the high-risk groups benefited more from ICIs than the low-risk groups, consistent with the results showing that the TMB was positively associated with the risk score. Currently, immunotherapy has emerged as an alternative therapy for patients with gliomas who cannot tolerate conventional treatments.[50] However, due to the inherent immunosuppressive microenvironment of gliomas and the low TMB in some patients, the effect of immunotherapy is unsatisfactory.[51–53] Therefore, the risk score we built might be used to stratify patients with gliomas, which might help clinicians choose more individualized and effective treatment methods for patients according to the risk score.

Next, the biological functions associated with the risk score were evaluated. Numerous pathways associated with metabolic processes, tumor progression, the epithelial-mesenchymal transition (EMT), extracellular matrix (ECM) and stromal cell-related functions were identified in the high-risk groups using the KEGG and gene ontology analyses. Fibroblasts have been shown to inhibit the immune response and promote tumor development, and osteoblasts have been found to promote tumor metastasis.[54,55] ECM signaling has been reported to inhibit tumor cell apoptosis and increase the ability of cells to proliferate and infiltrate.[56]

Finally, some limitations of our study must be addressed. First, no mutation data were available in the CGGA database, which prevented us from calculating the TMB of the CGGA samples. Second, this study was a retrospective study conducted using public databases. Prospective studies should be conducted as a supplement in the future. Third, the level of infiltrating immune cells, drug sensitivity and biological functions must be further confirmed by performing in vitro experiments and large-scale clinical trials.

5. Conclusions

Dysregulated lipid metabolism is one of the novel hallmarks of tumors. A lipid metabolism-related risk signature might effectively assess the prognosis of patients with gliomas. The risk score was significantly correlated with the prognosis, immune features, drug sensitivity and biological molecular functions, which has important implications for the decision making of clinicians and individualized treatment of patients with gliomas.

Author contributions

Conceptualization: Ting Liu.
Data curation: Dingqiang Meng and Ting Liu.
Formal analysis: Dingqiang Meng and Ting Liu.
Methodology: Ting Liu.
Project administration: Dingqiang Meng and Ting Liu.
Resources: Ting Liu.
Software: Dingqiang Meng and Ting Liu.
Support: Dingqiang Meng and Ting Liu.
Writing – original draft: Dingqiang Meng and Ting Liu.
Writing – review & editing: Dingqiang Meng and Ting Liu.
Data curation: Dingqiang Meng, Ting Liu.
Formal analysis: Dingqiang Meng, Ting Liu.
Investigation: Dingqiang Meng.
Methodology: Dingqiang Meng, Ting Liu.
Resources: Dingqiang Meng.
Software: Dingqiang Meng, Ting Liu.
Supervision: Dingqiang Meng.
Writing – original draft: Dingqiang Meng, Ting Liu.
Writing – review & editing: Dingqiang Meng, Ting Liu.

Correction

The corresponding author information has been corrected from "Department of Neurology, Traditional Chinese Medicine Hospital, Bachuan Street, TongLiang District, ChongQing 402560" to "Department of Neurology, Traditional Chinese Medicine Hospital. Tongliang. Chongqing. Chongqing, China. post code: 402560."

References

[1] Li W, Xu M, Li Y, et al. Comprehensive analysis of the association between tumor glycolysis and immune/inflammation function in breast cancer. J Transl Med. 2020;18:92.
[2] Hamaidi I, Zhang L, Kim N, et al. Sirt2 inhibition enhances metabolic fitness and effector functions of tumor-reactive T cells. Cell Metab. 2020;32:420–436.e12.
[3] Merino Salvador M, Gómez de Cedrón M, Moreno Rubio J, et al. Lipid metabolism and lung cancer. Crit Rev Oncol Hematol. 2017;112:31–40.
[4] Cheng C, Geng F, Cheng X, et al. Lipid metabolism reprogramming and its potential targets in cancer. Cancer Commun (Lond). 2018;38:27.
[5] Santos CR, Schulze A. Lipid metabolism in cancer. FEBS J. 2012;279:2610–23.
[6] Gao X, Zhao N, Dong L, et al. A novel lipid prognostic signature of ADCY2, LIPE, and OLR1 in head and neck squamous cell carcinoma. Front Oncol. 2021;11:735993.
[7] Cao Y. Adipocyte and lipid metabolism in cancer drug resistance. J Clin Invest. 2019;129:3006–17.
[8] Liu Q, Luo Q, Halim A, et al. Targeting lipid metabolism of cancer cells: a promising therapeutic strategy for cancer. Cancer Lett. 2017;401:39–45.
[9] Cheng C, Geng F, Cheng X, et al. Lipid metabolism reprogramming and its potential targets in cancer. Cancer Commun (lond). 2018;38:27–40.
[10] Zhu K, Xiaoqiang L, Deng W, et al. Development and validation of a novel lipid metabolism-related gene prognostic signature and candidate drugs for patients with bladder cancer. Lipids Health Dis. 2021;20:146–164.
[11] Broadfield LA, Pane AA, Talebi A, et al. Lipid metabolism in cancer: new perspectives and emerging mechanisms. Dev Cell. 2021;56:1363–93.
[12] Harbuzariu A, Gonzalez-Perez RR. Leptin-Notch axis impairs 5-fluorouracil effects on pancreatic cancer. Oncotarget. 2018;9:18239–53.
[13] Bartucci M, Svensson S, Ricci-Vitiani L, et al. Obesity hormone leptin induces growth and interferes with the cytotoxic effects of 5-fluorouracil in colorectal tumor stem cells. Endocr Relat Cancer. 2010;17:823–33.
[14] Zhuo S, Chen Z, Yang Y, et al. Clinical and biological significances of a ferroptosis-related gene signature in gliomas. Front Oncol. 2020;10:590861.
[15] Gilbert MR, Dignam JJ, Armstrong TS, et al. A randomized trial of bevacizumab for newly diagnosed glioblastoma. N Engl J Med. 2014;370:699–708.
[16] Aldape K, Brindle KM, Chesler L, et al. Challenges to curing primary brain tumours. Nat Rev Clin Oncol. 2019;16:509–20.
[17] Wan RJ, Peng W, Xia QX, et al. Ferroptosis-related gene signature predicts prognosis and immunotherapy in gliomas. CNS Neurosci Ther. 2021;27:973–86.

[18] Cirillo A, Di Salle A, Petillo O, et al. High grade glioblastoma is associated with aberrant expression of ZFP57, a protein involved in gene imprinting, and of CPT1A and CPT1C that regulate fatty acid metabolism. Cancer Biol Ther. 2014;15:735–741.
[19] Sun P, Xia S, Lal B, et al. Lipid metabolism enzyme ACSVL3 supports glioblastoma stem cell maintenance and tumorigenicity. BMC Cancer. 2014;14:401.
[20] Grube S, Dünisch P, Freitag D, et al. Overexpression of fatty acid synthase in human gliomass correlates with the WHO tumor grade and inhibition with Orlistat reduces cell viability and triggers apoptosis. J Neurooncol. 2014;118:277–87.
[21] Jiang P, Gu S, Pan D, et al. Signatures of T cell dysfunction and exclusion predict cancer immunotherapy response. Nat Med. 2018;24:1550–8.
[22] Yoshihara K, Shahmoradgoli M, Martínez E, et al. Inferring tumour purity and stromal and immune cell admixture from expression data. Nat Commun. 2013;4:2612.
[23] Newman AM, Liu CL, Green MR, et al. Robust enumeration of cell subsets from tissue expression profiles. Nat Methods. 2015;12:453–7.
[24] Geeleher P, Cox N, Huang RS. pRRophetic: an R package for prediction of clinical chemotherapeutic response from tumor gene expression levels. PLoS One. 2014;9:e107468.
[25] Justus CR, Sanderlin EJ, Yang LV. Molecular connections between cancer cell metabolism and the tumor microenvironment. Int J Mol Sci. 2015;16:11055–86.
[26] Fu Y, Sun S, Bi J, et al. An HDAC9-associated immune-related signature predicts bladder cancer prognosis. PLoS One. 2022;17:e0264527.
[27] Guo D, Reinitz F, Youssef M, et al. An LXR agonist promotes glioblastoma cell death through inhibition of an EGFR/AKT/SREBP-1/LDLR-dependent pathway. Cancer Discov. 2011;1:442–56.
[28] Offer S, Menard JA, Pérez JE, et al. Extracellular lipid loading augments hypoxic paracrine signaling and promotes gliomas angiogenesis and macrophage infiltration. J Exp Clin Cancer Res. 2019;38:241.
[29] Pei Z, Sun P, Huang P, et al. Acyl-CoA synthetase VL3 knockdown inhibits human gliomas cell proliferation and tumorigenicity. Cancer Res. 2009;69:9175–82.
[30] He Z, Wang C, Xue H, et al. Identification of a metabolism-related risk signature associated with clinical prognosis in glioblastoma using integrated bioinformatic analysis. Front Oncol. 2020;10:1631–45.
[31] Qi Y, Chen D, Lu Q, et al. Bioinformatic profiling identifies a fatty acid metabolism-related gene risk signature for malignancy, prognosis, and immune phenotype of gliomas. (1875-8630 (Electronic)).
[32] Zhang CA-O, Wang MA-O, Ji FA-O, et al. A novel glucose metabolism-related gene signature for overall survival prediction in patients with glioblastoma. (2314-6141 (Electronic)).
[33] Lee HY, Nam Y, Choi WS, et al. The hepato-protective effect of eupatilin on an alcoholic liver disease model of rats. Korean J Physiol Pharmacol. 2020;24:385–94.
[34] Molina-Ortiz D, Camacho-Carranza R, González-Zamora JF, et al. Differential expression of cytochrome P450 enzymes in normal and tumor tissues from childhood rhabdomyosarcoma. PLoS One. 2014;9:e93261.
[35] Man XB, Tang L, Qiu XH, et al. Expression of cytochrome P4502E1 gene in hepatocellular carcinoma. World J Gastroenterol. 2004;10:1565–8.
[36] Ladero JM, Agúndez JA, Rodríguez-Lescure A, et al. RsaI polymorphism at the cytochrome P4502E1 locus and risk of hepatocellular carcinoma. Gut. 1996;39:330–3.
[37] Ye L, Xu Y, Wang L, et al. Downregulation of CYP2E1 is associated with poor prognosis and tumor progression of gliomass. Cancer Med. 2021;10:8100–13.
[38] Bellmunt J, Powles T, Vogelzang NJ. A review on the evolution of PD-1/PD-L1 immunotherapy for bladder cancer: the future is now. Cancer Treat Rev. 2017;54:58–67.
[39] Bi Y, Wu ZH, Cao F. Prognostic value and immune relevancy of a combined autophagy-, apoptosis- and necrosis-related gene signature in glioblastoma. BMC Cancer. 2022;22:233.
[40] Huang L, Wang Z, Chang Y, et al. EFEMP2 indicates assembly of M0 macrophage and more malignant phenotypes of gliomas. Aging (Albany NY). 2020;12:8397–412.
[41] Qi Y, Yang X, Ji C, et al. Identification of an IL-4-Related Gene Risk Signature for Malignancy, Prognosis and Immune Phenotype Prediction in Glioma. Brain Sci. 2022;12:181–93.
[42] Rahbar A, Cederarv M, Wolmer-Solberg N, et al. Enhanced neutrophil activity is associated with shorter time to tumor progression in glioblastoma patients. Oncoimmunology. 2016;5:e1075693.
[43] Girndt M, Trojanowicz B, Ulrich C. Monocytes in Uremia. Toxins (Basel). 2020;12:340–59.
[44] Perus LJM, Walsh LA. Microenvironmental heterogeneity in brain malignancies. Front Immunol. 2019;10:2294–308.
[45] Wherry EJ, Kurachi M. Molecular and cellular insights into T cell exhaustion. Nat Rev Immunol. 2015;15:486–99.
[46] Li M, Li G, Kiyokawa J, et al. Characterization and oncolytic virus targeting of FAP-expressing tumor-associated pericytes in glioblastoma. Acta Neuropathol Commun. 2020;8:221.
[47] Wang X, Ye L, He W, et al. In situ targeting nanoparticles-hydrogel hybrid system for combined chemo-immunotherapy of gliomas. J Control Release. 2022;345:786–97.
[48] Chen Z, Wu T, Yan Z, et al. Identification and validation of an 11-ferroptosis related gene signature and its correlation with immune checkpoint molecules in gliomas. Front Cell Dev Biol. 2021;9:652599.
[49] Samstein RM, Lee CH, Shoushtari AN, et al. Tumor mutational load predicts survival after immunotherapy across multiple cancer types. Nat Genet. 2019;51:202–6.
[50] Xu S, Tang L, Li X, et al. Immunotherapy for gliomas: current management and future application. Cancer Lett. 2020;476:1–12.
[51] Bouffet E, Larouche V, Campbell BB, et al. Immune checkpoint inhibition for hypermutant glioblastoma multiforme resulting from germline biallelic mismatch repair deficiency. J Clin Oncol. 2016;34:2206–11.
[52] Touat M, Li YY, Boynton AN, et al. Mechanisms and therapeutic implications of hypermutation in gliomass. Nature. 2020;580:517–23.
[53] Pombo Antunes AR, Scheyltjens I, Duerinck J, et al. Understanding the glioblastoma immune microenvironment as basis for the development of new immunotherapeutic strategies. Elife. 2020;9.
[54] Monteran L, Erez N. The dark side of fibroblasts: cancer-associated fibroblasts as mediators of immunosuppression in the tumor microenvironment. Front Immunol. 2019;10:1835.
[55] Riquelme MA, Cardenas ER, Jiang JX. Osteocytes and bone metastasis. Front Endocrinol (Lausanne). 2020;11:567844.
[56] Walker C, Mojares E, Del Río Hernández A. Role of extracellular matrix in development and cancer progression. Int J Mol Sci. 2018;19.